Autotrack Control Systems for Antenna Mounts with Non-Orthogonal Axes

By W. L. NELSON and W. J. COLE

(Manuscript received May 17, 1965)

The use of non-orthogonal, or conic, mounts for steerable antennas introduces some control system design problems not present in the more conventional orthogonal mounts. These problems result from both the geometrical and the mechanical cross-coupling which occurs between the two non-orthogonal axes of motion.

This paper presents a general analysis and design of the control system for the open cassegrain antenna which can be readily applied to other non-orthogonal antenna structures. The form of the feedback controller for approximately non-interacting control of each axis is developed. Also described is a supplementary control strategy for providing tracking near the zenith region without excessively high slewing rates.

A computer simulation of the system has verified the basic control strategy for non-orthogonal mounts and established the feasability of operating compact antenna structures such as the open cassegrain design under severe wind conditions without a radome.

I. GENERAL SYSTEM DESCRIPTION

While the general control system design methods developed in this study apply to any antenna mount using two non-orthogonal axes, the specific structure considered throughout this paper is the slant-mounted open-cassegrain antenna.[1] In this structure, the antenna beam tracks the target by controlled rotational motion about the inclined and the vertical axes shown in Fig. 1. While motion about the vertical axis produces true azimuth motion of the beam, the motion about the inclined axis generates a combination of azimuth and elevation motion of the beam. Further cross-coupling between the azimuth and elevation tracking channels is introduced by unavoidable mechanical coupling of motion between the two drive axes.

Fig. 2 is a general block diagram of the tracking control system. The

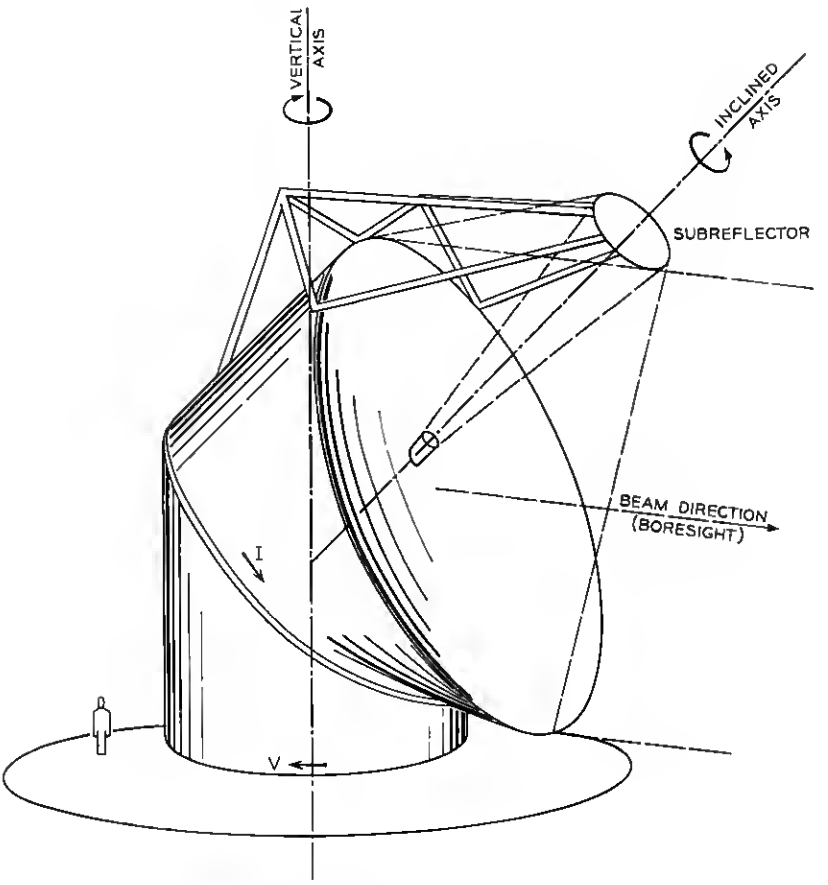

Fig. 1 — Open cassegrain antenna with two-axis conic mount structure showing simplified subreflector structure.

pointing error is resolved for convenience into the standard azimuth and elevation angle errors (this is a conceptual, not physical, portion of the system). In the tracking of active repeater satellites, the error signals are derived from the waveguide mode detector receiving the satellite beacon signal.[2] The horizontal and vertical error signals, ϵ_h and ϵ_v, at the output of the error detector are related to the azimuth and elevation errors by

$$\begin{aligned} \epsilon_h &= K_h \, (\cos E)(A_r - A) \\ \epsilon_v &= K_v(E_r - E) \end{aligned} \tag{1}$$

where K_h and K_v are the detector gains, A_r and E_r are the reference azimuth and elevation angles, respectively, of the satellite, and A and E are the controlled azimuth and elevation angles of the beam axis (electrical boresight) of the antenna.

All of the equations of motion of the antenna drive system and physical structure (considered in detail in Section III) can be represented here by the single nonlinear differential equation,

$$\frac{d\mathbf{W}}{dt} = \mathbf{F}(\mathbf{W},\mathbf{u}) \tag{2}$$

where $\mathbf{W}$ is the state vector containing as components those variables necessary to adequately represent the dynamics of the antenna system, and $\mathbf{F}$ is the vector-valued function relating the time derivative of the state to itself and to the control vector, $\mathbf{u}$ (with components u_1 and u_2).

From the error signals (1), as well as from feedback signals derived from the components of the state vector, $\mathbf{W}$, the controller must generate the two antenna drive signals, u_1 and u_2, which control the antenna angles, V and I, in such a way as to reduce the tracking error and keep the antenna beam automatically "locked-on" to the satellite. Because of the complex, nonlinear, multivariate nature of this system, the design of the controller cannot be achieved by conventional analytic design methods. A preliminary controller design, based on a linear approximation of the system dynamics, together with the appropriate coordinate transformations and supervisory control logic, is discussed in Section IV. The final design will be evolved from this preliminary design through an

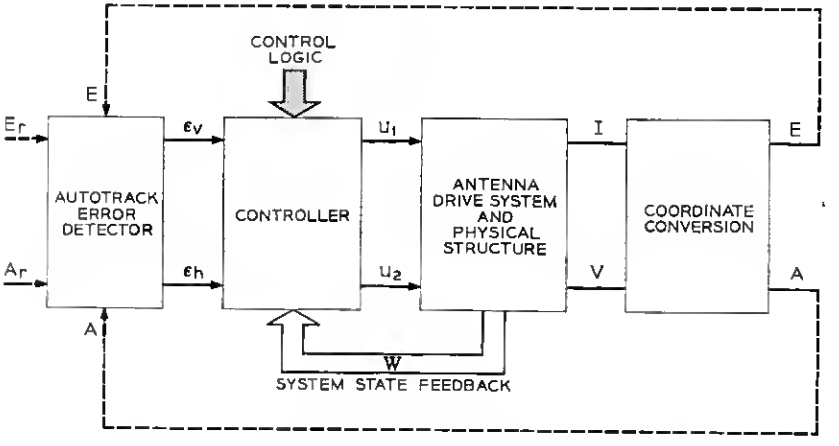

Fig. 2 — Preliminary block diagram for antenna control system.

accurate computer simulation of the overall system, its inputs, and its environment.

II. CONIC MOUNT CHARACTERISTICS

To gain an initial understanding of the tracking requirements on this system, the basic transformations between the antenna angles (I,V) and the tracking angles (E,A) are needed. Some of this is similar to a study on conic mounts by Norton,[3] and his notation is used here.

Fig. 3 shows the geometry of the conic mount, in particular the structural design angles (α,β), the inclined- and vertical-axis angles (I,V), and the elevation and azimuth angles (E,A).

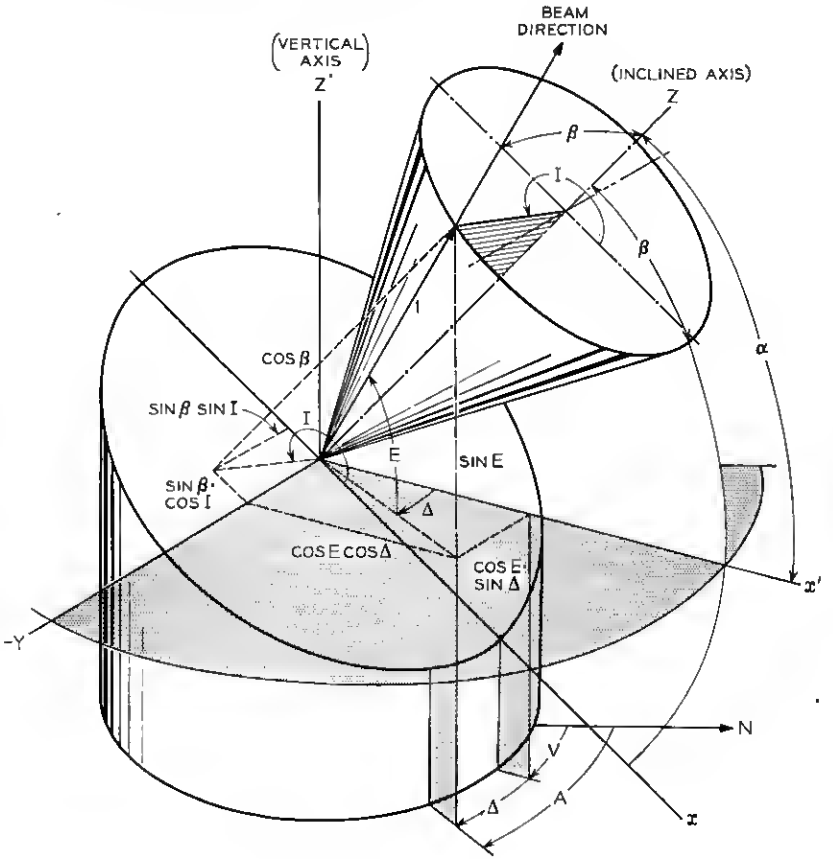

Fig. 3 — Conic mount geometry.

Since V produces only azimuth motion, the only coordinate conversions needed are those giving the azimuth angle Δ and the elevation angle E produced by I. Fig. 3 indicates that these angles are related by rotation about the y-axis through an angle $(90° - \alpha)$, which corresponds to the rectangular coordinate transformation:

$$\begin{pmatrix} x' \\ y' \\ z' \end{pmatrix} = \begin{pmatrix} \sin \alpha & 0 & \cos \alpha \\ 0 & 1 & 0 \\ -\cos \alpha & 0 & \sin \alpha \end{pmatrix} \begin{pmatrix} x \\ y \\ z \end{pmatrix}. \tag{3}$$

For a unit radius, the spherical coordinate equivalents of these rectangular coordinates are,

$$\begin{pmatrix} \cos E \cos \Delta \\ -\cos E \sin \Delta \\ \sin E \end{pmatrix} = \begin{pmatrix} \sin \alpha & 0 & \cos \alpha \\ 0 & 1 & 0 \\ -\cos \alpha & 0 & \sin \alpha \end{pmatrix} \begin{pmatrix} \sin \beta \cos I \\ \sin \beta \sin I \\ \cos \beta \end{pmatrix}. \tag{4}$$

Multiplying out the right-hand side of (4), the coordinate conversions can be expressed as

$$\begin{aligned} E &= \sin^{-1} (\sin \alpha \cos \beta - \cos \alpha \sin \beta \cos I) \\ \Delta &= \tan^{-1} \left[\frac{-\sin \beta \sin I}{\cos \alpha \cos \beta + \sin \alpha \sin \beta \cos I} \right] \\ A &= V + \Delta. \end{aligned} \tag{5}$$

In order to have complete coverage of the zenith region, it is necessary that $E = 90°$ when $I = 180°$. From (5) this occurs if and only if $\alpha + \beta = 90°$. All relationships from here on assume this zenith condition. In particular, since $\alpha + \beta = 90°$, let us define,

$$\left.\begin{aligned} a &\equiv \sin \alpha = \cos \beta \\ b &\equiv \sin \beta = \cos \alpha \end{aligned}\right\} a^2 + b^2 = 1 \tag{6}$$

so the elevation-azimuth expressions (5) reduce to*

* The antenna mount for the open cassegrain design[1] has $\alpha = 42.5°$ and $\beta = 47.5°$ which gives a $-5°$ to $90°$ range in E. Therefore $\sin \alpha = \cos \beta = 0.67559$, and $\sin \beta = \cos \alpha = 0.73728$, but for simplicity of notation, and somewhat more generality, we continue to use a and b.

$$\begin{aligned} E &= \sin^{-1}(a^2 - b^2 \cos I) \\ \Delta &= \tan^{-1}\left[-\frac{1}{a}\tan\left(\frac{I}{2}\right)\right] \\ A &= V + \Delta. \end{aligned} \tag{7}$$

The inverse of these expressions gives the required antenna mount angles, I and V, to produce a given azimuth and elevation of the beam axis:

$$\begin{aligned} I &= \cos^{-1}\left(\frac{a^2 - \sin E}{1 - a^2}\right) \\ V &= A - \Delta \\ \Delta &= -\sigma(I)\tan^{-1}\left(\frac{1}{a}\sqrt{\frac{1 - 2a^2 + \sin E}{1 - \sin E}}\right) \end{aligned} \tag{8}$$

where we define

$$\sigma(I) \equiv \operatorname{sgn}(\sin I) \equiv \frac{\sin I}{|\sin I|}. \tag{9}$$

These relationships between the angles I, $\Delta = A - V$, and E are plotted in rectangular form in Fig. 4, and in polar form in Fig. 5. It is apparent from these figures that there are two pairs of drive angles (I,V) corresponding to every pair of tracking angles (E,A).* However, in continuous tracking of a moving target, the choice of which pair (I,V) to use in pointing the antenna to the given (E,A) is arhitrary only at the heginning of the track, since instantaneous switchover to the opposite pair is not possihle. To switch from one pair to the other may he necessary or desirable in certain applications (see Section 4.2), but it can bc accomplisbed only by moving the antenna horesigbt off the target for some finite period of time. The exception to this is the unique case of the target track which passes precisely through the zenith, at which instant the two (I,V) pairs coincide, so that instantaneous switchovcr can be made.

Finally, the coordinatc conversions between the conic mount angular velocities $(\dot{I},\dot{V})$ and the tracking angular velocities $(\dot{E},\dot{A})$ are of interest in determining the control system requirements. Using (6), (8), and (9) we get

* For example, for the tracking angles ($E = 40°$, $A = 80°$), there are the two equivalent pairs of drive angles ($I_1 = 110°$, $V_1 = 145°$) and ($I_2 = 250°$, $V_2 = 15°$).

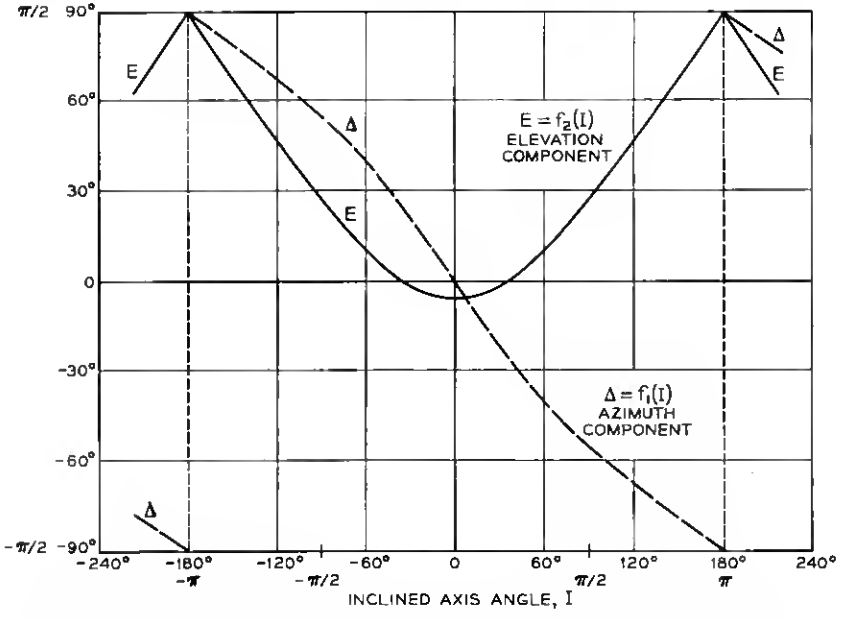

Fig. 4 — Resolution of inclined axis angle into elevation and azimuth components for antenna parameters: $\alpha = 42.5°$, $\beta = 47.5°$.

$$\begin{aligned} \dot{I} &= \sigma(I)\left(1 - \frac{2a^2}{1 + \sin E}\right)^{-\frac{1}{2}} \dot{E} \\ \dot{\Delta} &= -\frac{a\dot{I}}{1 + a^2 - b^2 \cos I} + \pi\delta\left(\cos\frac{I}{2}\right) \\ \dot{V} &= \dot{A} - \dot{\Delta} \end{aligned} \tag{10}$$

where δ $(\cos I/2)$ is the Dirac delta function of $(\cos I/2)$, representing the derivative of the step discontinuity in Δ which occurs whenever $\cos(I/2) = 0$, i.e., whenever $I = \pm(2n + 1)\pi$, $n = 0,1,2, \cdots$ (see Fig. 4).

To predict the tracking requirements for the two-axis conic mount, it is clear from (8) and (10) that the elevation and azimuth angles (E,A), and rates $(\dot{E},\dot{A})$ are needed. In the tracking of communication satellites, these are functions of the orbit parameters of the satellites, the locations of the tracking station, and the time reference chosen. Computer routines for providing such data are available.[4] For the purpose of analysis and preliminary design, however, it is desirable to have

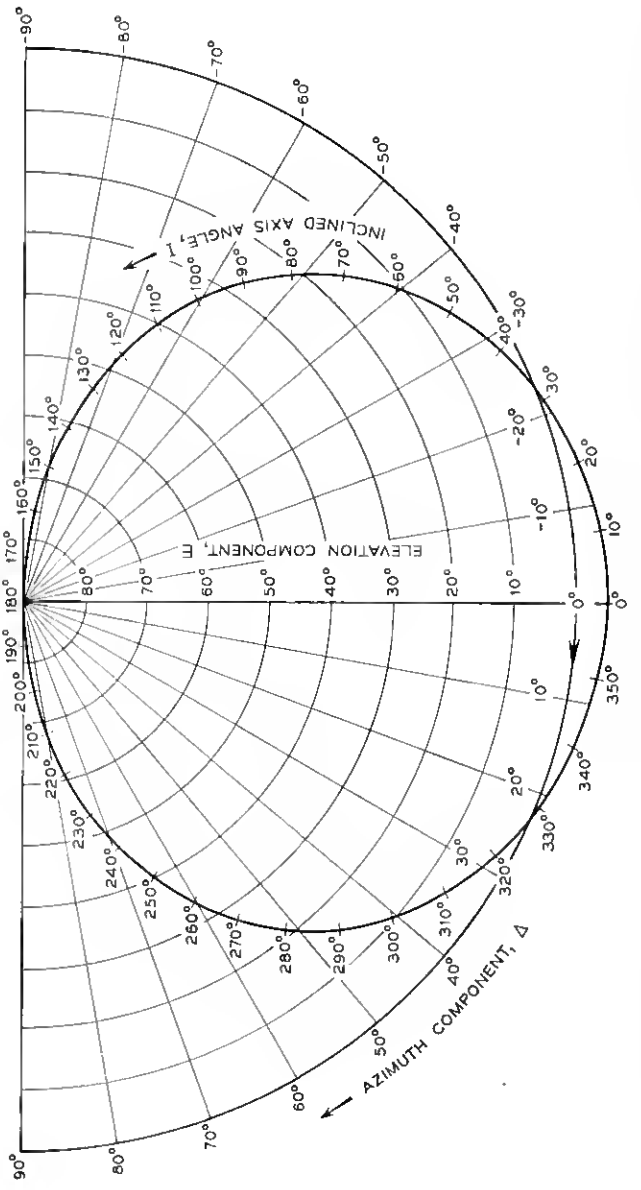

Fig. 5 — Polar plot of azimuth and elevation components of the inclined axis angle for antenna with parameters $\alpha = 42.5°, \beta = 47.5°$.

analytic expressions for the azimuth and elevation angles and rates for circular orbits. These expressions are derived in Appendix A.

III. DYNAMICAL MODEL OF ANTENNA AND DRIVE MOTORS

As an essential step in the design of the control system, we consider now the mathematical model of the antenna mechanical system and the drive motors. Although the model must realistically represent the output angle response (I,V) to input signals, (u_1, u_2), some simplification will be made to ease computer simulation.

The model of the antenna mechanical system, based on a study by Coyne,[5] which was considered to adequately represent the essential dynamics, is illustrated in Fig. 6.

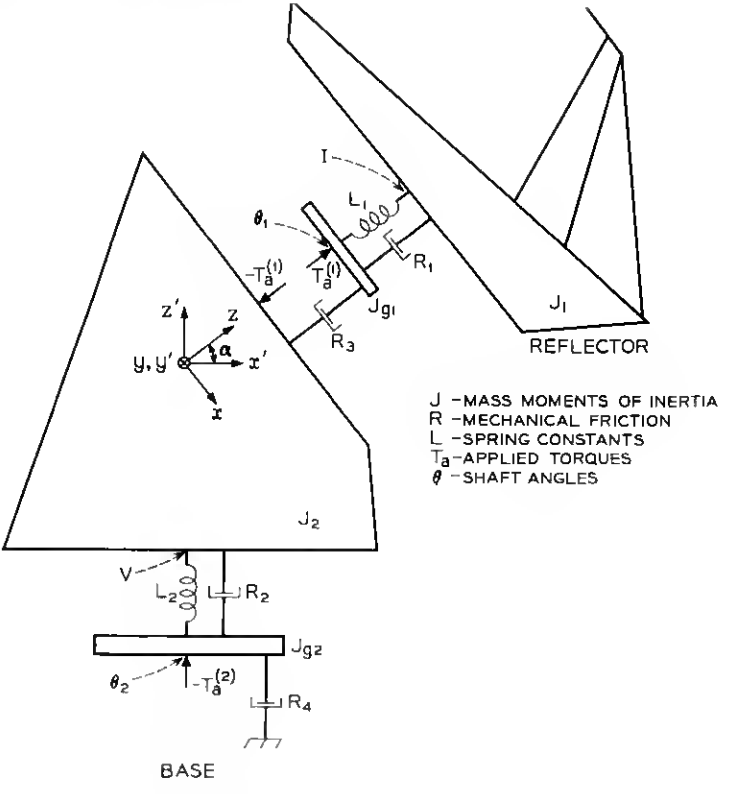

Fig. 6 — Model of antenna mechanical system.

Using the notation in Fig. 6, the equations of motion are

$$T_a^{(1)} = J_{g1}\ddot{\theta}_1 + L_1(\theta_1 - I) + R_1(\dot{\theta}_1 - \dot{I}) + R_3\dot{\theta}_1 \tag{11}$$
$$L_1(\theta_1 - I) + R_1(\dot{\theta}_1 - \dot{I}) = J_{1zz}\ddot{I} - m_1 ,$$

for the reflector structure, and

$$T_a^{(2)} = J_{g2}\ddot{\theta}_2 - L_2(V - \theta_2) - R_2(\dot{V} - \dot{\theta}_2) + R_4\dot{\theta}_2 \tag{12}$$
$$-L_2(V - \theta_2) - R_2(\dot{V} - \dot{\theta}_2) = J_{2z'z'}\ddot{V} - aT_a^{(1)} + m_2 ,$$

for the base structure, where

$$\begin{aligned} m_1 &= -bJ_{1xz}(\ddot{V}\cos I - \dot{I}\dot{V}\sin I) + aJ_{1zz}\ddot{V}, \\ m_2 &= b^2 J_{1yy}\sin I(\ddot{V}\sin I + \dot{I}\dot{V}\cos I) \\ &\quad + b\cos I[J_{1xx}b(\ddot{V}\cos I - \dot{I}\dot{V}\sin I) - J_{1xz}(a\ddot{V} - \ddot{I})]. \end{aligned} \tag{13}$$

The product mass moments of inertia of the reflector section are defined with respect to the x-y-z coordinate system. The $J_{2z'z'}$ is measured with respect to the vertical (z') axis.

Due to the large speed variations required in tracking, and because a stiff drive is needed to cope with disturbance torques, it is expected that hydraulic transmissions similar to the units used to drive the Andover horn-reflector antenna[6] will be employed as the drive units. In addition, direct gearing is assumed.

The differential equation which describes the hydraulic drive unit[6] is

$$K_u u = K_m\dot{\theta}_m + K_L P + K_C\dot{P} \tag{14}$$

where u, θ_m, and P represent the drive signal from the controller, motor shaft angle, and hydraulic pressure. The torque delivered by the hydraulic unit is proportional to the pressure, or

$$T_D = K_T P. \tag{15}$$

Equation (14) is valid provided the pressure, P, is less than the maximum pressure, $P_{\max}$, which is allowed in the transmission. This condition is shown in Fig. 7 where the lines AB and CD represent (14) with $u = \pm\bar{v}_{\max}$ and AD and BC represent $P = \pm P_{\max}$. The line EOF represents the operating line or static load line of the hydraulic transmission. To illustrate the dynamic operating of the hydraulic transmission, suppose the operating point is at G with $u = \bar{v}_2$ and a large change in drive signal to $u = \bar{v}_1$ occurs. The motor velocity cannot change instantaneously, so that the pressure in the transmission unit becomes larger. If the drive signal change is large enough, the P may exceed $P_{\max}$ and the

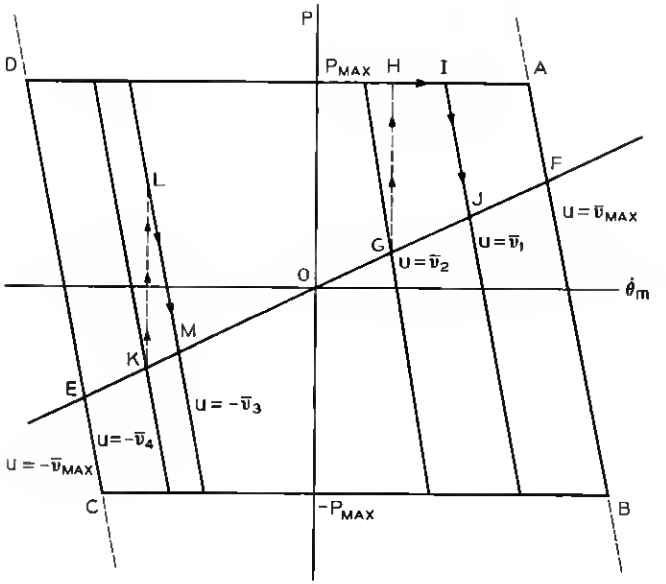

Fig. 7 — Dynamic operation of hydraulic transmission.

new operating point jumps to point H in Fig. 7. At this point, a relief valve is actuated which maintains the pressure at $P_{\max}$ and the torque at $K_T P_{\max}$ until the shaft velocity increases to the value at point I. Then, (14) is again valid with $u = \bar{v}_1$ and the shaft velocity will increase to the value at J. If the drive signal change is such that $P < P_{\max}$, the dynamic path is similar to KLM. As a result, in the system simulation, the value of P must be monitored and, if it exceeds $P_{\max}$, we must set $P = P_{\max}$, i.e., a limiting function.

A counter-torque arrangement of the motors was assumed to eliminate hysteresis effects in the drive systems.[6] This permits the linear gear train equations,

$$\begin{aligned} T_a &= N_G T_D , \\ \theta_m &= N_G \theta , \end{aligned} \tag{16}$$

to apply, where T_a, θ, and N_G are the torque applied to each axis in Fig. 6, the shaft angle at the gearhox output, and the gear ratio, respectively.

The mathematical model for the computer simulation of the antenna structure and the drive motors, represented by (11) through (16) and Fig. 7, is shown in detailed block diagram form in Figs. 8 and 9.

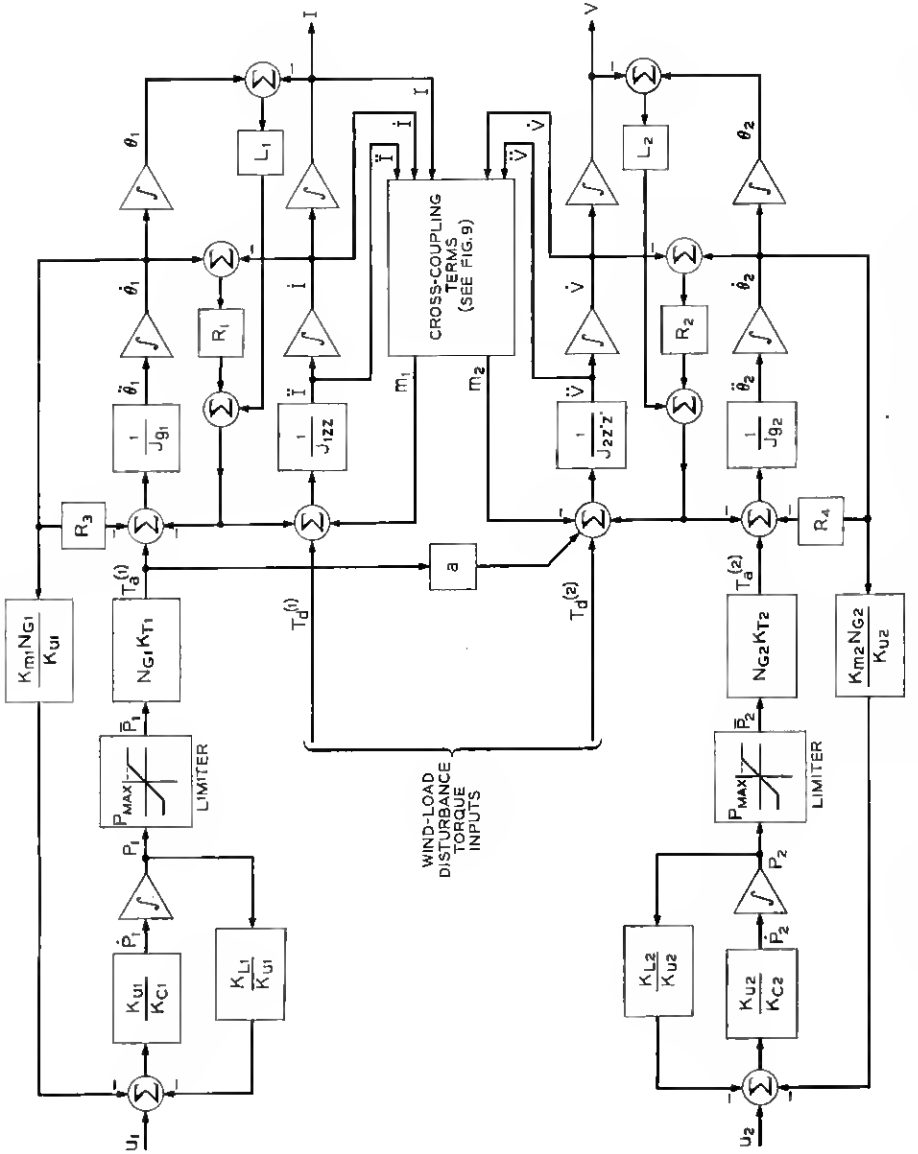

Fig. 8 — Block diagram of equations of motion of antenna structure in response to drive torques.

IV. CONTROLLER DESIGN

4.1 *Approximately Non-Interacting Control*

In order to design the controller for approximately non-interacting control of each channel, it is necessary first to represent the drive motors and antenna structure in terms of a linear system which is a good approximation of the actual system in the small error-signal case and normal operating conditions. We assume first that the drive motors are unsaturated, i.e. $P < P_{max}$. Next we assume that the torsional spring constants of the reflector and base structures are sufficiently large that $\theta_1(t) \doteq I(t)$ and $\theta_2(t) \doteq V(t)$.

Although these assumptions linearize and simplify the drive and self-coupling portion of each channel in Fig. 8, some major complexities and nonlinearities of the system remain in the cross-coupling portion shown in Fig. 9. There are, unfortunately, no reasonable or standard assumptions to apply to this portion, only educated guesses. After examining the relative magnitude of the various terms in Fig. 9 for typical satellite tracks, the simplified linear system representation shown in Fig. 10 was chosen for the preliminary design study.

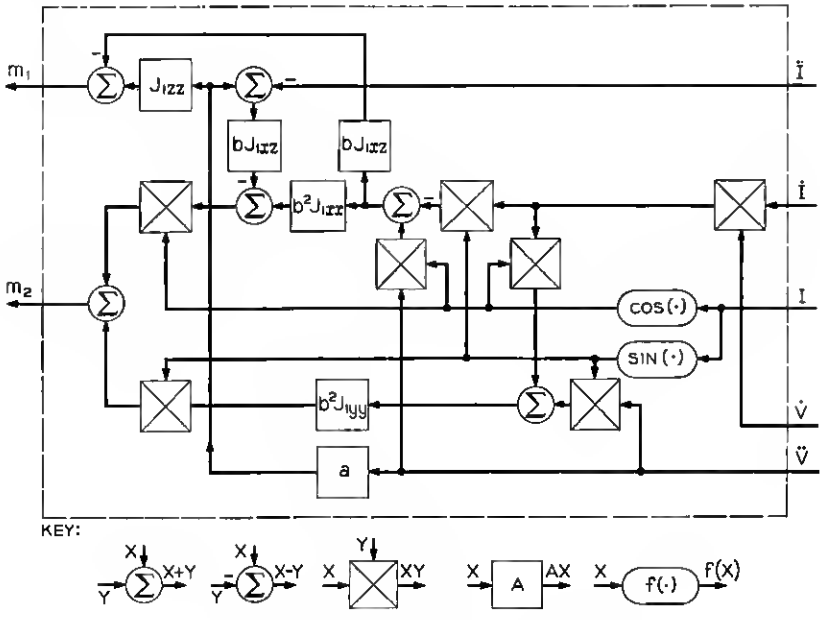

Fig. 9 — Cross coupling portion of Fig. 8.

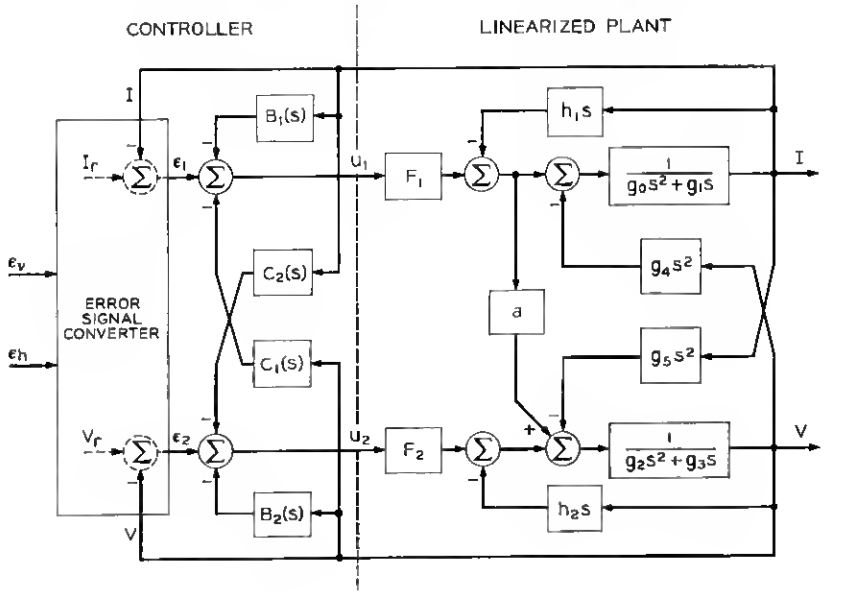

Fig. 10 — Simplified linear system representation for deriving basic non-interacting controller.

Fig. 10 also shows the elements of the basic controller design: the error signal conversion unit and the feedbaek compensation units.

The channel error signals, whieh are eonceptually shown in Fig. 10 as the difference between the desired, or reference, angle and the output angle for each channel, are obtained as physical signals from the eonversion of the autotraek error signals, given in (1). This conversion, derived in Appendix B under the assumption of small errors, is given by,

$$\begin{aligned} \epsilon_1 &\doteq \frac{1}{K_v}\left[1 + a^2 \operatorname{eot}^2 \frac{I}{2}\right]\epsilon_v \\ \epsilon_2 &\doteq \left[\frac{a}{2K_v}\csc^2\frac{I}{2}\right]\epsilon_v + \left[K_h b^2 \sin^2 I\left(1 + a^2\cot^2\frac{I}{2}\right)\right]^{-1}\epsilon_h , \end{aligned} \tag{17}$$

where K_v and K_h are the detector gains in (1), and the constants a and b are defined in (6).

The controller outputs, u_1 and u_2, are derived from these error signals plus additional compensation through the feedback networks $B(s)$ and $C(s)$. The purpose of these networks is to improve the response to errors in the same channel, and to eliminate the undesired response to errors in the opposite channel. For the development of this non-interacting

design it is convenient to use matrix notation. We define the input, output and control vectors,

$$\varphi_r = \begin{pmatrix} I_r \\ V_r \end{pmatrix}, \qquad \varphi = \begin{pmatrix} I \\ V \end{pmatrix}, \qquad \mathbf{u} = \begin{pmatrix} u_1 \\ u_2 \end{pmatrix}.$$

The overall input-output relationship is denoted by

$$\varphi(s) = D\varphi_r(s) \tag{18}$$

where, for non-interacting channels, the transfer matrix must be diagonal. Therefore, we require D to have the form

$$D = \begin{pmatrix} D_1(s) & 0 \\ 0 & D_2(s) \end{pmatrix}. \tag{19}$$

From the block diagram of Fig. 10, we obtain the intermediate relationships,

$$\begin{aligned} G\varphi(s) &= F\mathbf{u}(s) \\ \mathbf{u}(s) &= \varphi_r(s) - C\varphi(s), \end{aligned} \tag{20}$$

where

$$C = \begin{pmatrix} 1 + B_1(s) & C_1(s) \\ C_2(s) & 1 + B_2(s) \end{pmatrix}, \qquad F = \begin{pmatrix} F_1 & 0 \\ aF_1 & F_2 \end{pmatrix},$$

and (21)

$$G = \begin{pmatrix} g_0 s^2 + (g_1 + h_1)s & -g_4 s^2 \\ g_5 s^2 + a h_1 s & g_2 s^2 + (g_3 + h_2)s \end{pmatrix}.$$

Then, from (18) and (20), it follows that the controller matrix, C, is given by

$$C = D^{-1} - F^{-1}G. \tag{22}$$

Upon substitution of the matrices in (19) and (21) into (22), we obtain the required transfer functions of the controller units:

$$\begin{aligned} B_1(s) &= \frac{1}{D_1(s)} - 1 - \frac{1}{F_1}[g_0 s^2 + (g_1 + h_1)s] \\ B_2(s) &= \frac{1}{D_2(s)} - 1 - \frac{1}{F_2}[(g_2 + a g_4)s^2 + (g_3 + h_2)s] \\ C_1(s) &= \frac{1}{F_1}(g_4 s^2) \\ C_2(s) &= \frac{1}{F_2}[(a g_0 - g_5)\, s^2 + a g_1 s]. \end{aligned} \tag{23}$$

The only design objective incorporated in these controller functions is that of non-interacting channel control. This has fixed the cross-coupling controller units $C_1(s)$ and $C_2(s)$ in terms of the linear plant parameters, the output angles (I,V), and their derivatives. The self-coupling controller units, $B_1(s)$ and $B_2(s)$, however, depend not only on these plant parameters and state variables, but also on the choice of the channel input-output transfer functions, $D_1(s)$ and $D_2(s)$.

Since both $B_1(s)$ and $B_2(s)$ have the same functional form, we will use the subscript $i = 1,2$ to refer to either channel. From (23), $B_i(s)$ is written in the simplified form,

$$B_i(s) = \left(\frac{1}{D_i(s)} - 1\right) - \frac{s^2}{c_i} - \frac{s}{f_i}, \tag{24}$$

where for $i = 1$: $c_1 = F_1/g_0$, $\quad f_1 = F_1/(g_1 + h_1)$,

and for $i = 2$: $\quad c_2 = F_2/(g_2 + ag_4)$, $\quad f_2 = F_2/(g_3 + h_2)$.

Accuracy, fast response, stability, and a practical feedback structure are the general objectives which should be mutually satisfied to the extent possible in the choice of the channel transfer function, $D_i(s)$. More specifically, we consider the following requirements:

i. Each channel should have no steady-state error for step and ramp inputs.

ii. The feedback synthesis of $B_i(s)$ should employ signals proportional to the output angle, its velocity, and acceleration, but no higher derivatives.

iii. The error for a sinusoidal input, having an angular velocity no greater than ν_i and an acceleration no greater than γ_i, should not exceed the allowable value, ρ_i. (Appropriate numerical values of ν, γ, and ρ to be specified for each channel.)

iv. The choice of $D_i(s)$ should achieve a good compromise between the competitive aims of fast transient response and small noise bandwidth.

To satisfy requirements (i) and (ii), the channel transfer functions must be of the form

$$D_i(s) = \frac{c_i s + d_i}{s^3 + b_i s^2 + c_i s + d_i} \tag{25}$$

where the coefficient c_i is the same as in (24), but b_i and d_i are available as design parameters. Using (25) in (24) yields

$$B_i(s) = \frac{-1}{c_i s + d_i}\left[\left(\frac{d_i}{c_i} + \frac{c_i}{f_i} - b_i\right) s^2 + \frac{d_i}{f_i} s\right] \tag{26}$$

where c_i and f_i are defined below (24) in terms of the linear plant constants shown in Fig. 10.

The error transform for either channel is

$$\epsilon_i(s) = [1 - D_i(s)]\,\varphi_r(s) = \frac{s^2(s + b_i)\varphi_r(s)}{s^3 + b_i s^2 + c_i s + d_i} \tag{27}$$

where φ_r is the channel reference input (either I_r or V_r). Considering requirement (iii), φ_r is a sinusoidal signal,

$$\varphi_r(t) = \varphi_i(\omega) \sin \omega t,$$

where the peak amplitude is given by

$$\varphi_i(\omega) = \begin{cases} \nu_i/\omega, & \omega < \gamma_i/\nu_i \\ \gamma_i/\omega^2, & \omega \geqq \gamma_i/\nu_i \,. \end{cases} \tag{28}$$

The steady-state error for this input will not exceed the allowable value, ρ_i, provided

$$| 1 - D_i(j\omega) | \leqq \rho_i/\varphi_i(\omega) \,. \tag{29}$$

Both sides of (29) are shown in the log amplitude-log frequency plot of Fig. 11, using (28) and the asymptotic straight-line approximation of (27). Since at low frequencies,

$$| 1 - D_i(j\omega) | \doteq b_i\omega^2/d_i \,, \tag{30}$$

it follows that requirement (iii) imposes the design constraint (see Fig. 11),

$$b_i/d_i \leqq \rho_i/\gamma_i \tag{31}$$

which shows that for a given tolerable error, ρ_i, the limit on the parameter ratio is imposed by the peak acceleration, γ_i, rather than the peak velocity, ν_i.

In considering the transient response of each channel, we make use of a computer study made by J. F. Kaiser on the step and ramp response of the equivalent system

$$D(s) = \frac{\eta\omega_0^2 s + \omega_0^3}{s^3 + \mu\omega_0 s^2 + \eta\omega_0^2 s + \omega_0^3} \tag{32}$$

which has a noise bandwidth related to the coefficients by,

$$\mathfrak{B} \equiv \int_{-\infty}^{\infty} | D(j\omega) |^2 \, df = \frac{\eta^2 + \mu}{2(\eta\mu - 1)}\,\omega_0 \,. \tag{33}$$

From this study, the parameter values which seem to give the best com-

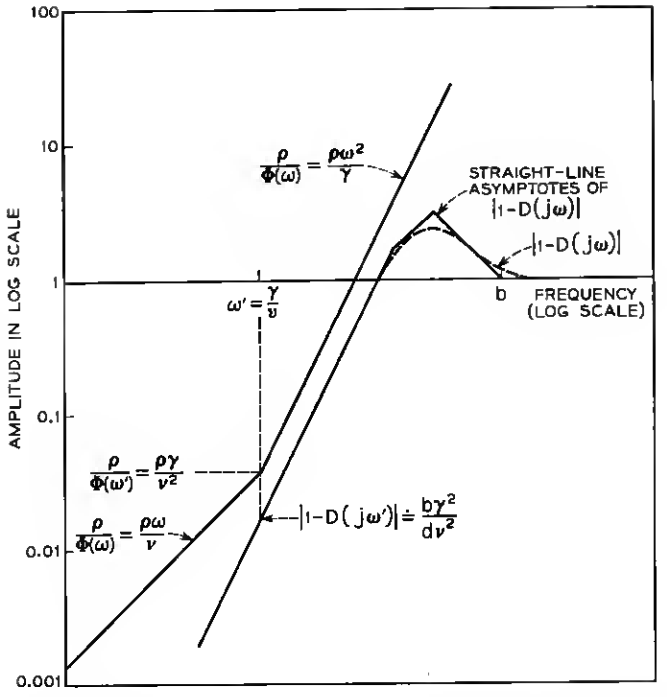

Fig. 11 — Amplitude-frequency sketch of error functions in relation (29).

promise between good transient response and small noise handwidth lie in the region,

$$\left.\begin{matrix} 2.3 < \eta < 2.7 \\ 1.8 < \mu < 2.3 \end{matrix}\right\} \tag{34}$$

within which the noise handwidth varies from ahout 0.9 ω_0 to 1.1 ω_0. For small handwidth, ω_0 should he chosen small. However, since $b_i = \mu\omega_0$ and $d_i = \omega_0^3$, the lower bound on ω_0 to satisfy (iii) is, from (31),

$$\omega_0^2 \geqq \mu(\gamma_i/\rho_i). \tag{35}$$

Furthermore, the choice of ω_0 is also linked to the physical system constants, since $c_i = \eta\omega_0^2$.

The detailed choice of the numerical values in the controller design cannot be made until all the values of the system constants and the operating requirements are known. However, the specific structure of the non-interacting controller designs can he given in terms of the channel gains F_1 and F_2, the plant parameters g_0 through g_5 (see Fig. 10), and

the variable parameters b_1, d_1, b_2 and d_2. This controller design for the normal autotrack mode of operation is shown in Fig. 12. The design of supplementary control action for special tracking modes is considered in the following section.

4.2 *Near Zenith Control Modes*

As noted in Section II, there are two possible tracking modes for a given satellite track. For later reference, let "mode 1" (I_1, V_1) be the tracking mode where $0 \leqq I \leqq 180°$ and "mode 2" (I_2, V_2) be the tracking mode where $180° \leqq I \leqq 360°$. These two modes are illustrated in Fig. 13 as a function of time for the tracking of a satellite in a circular equatorial orbit of 6000 miles altitude with the antenna site located at 2° latitude. As can be seen from this figure, the maximum vertical axis angular velocity required to stay on track, which we shall call $\dot{V}_{max}$, occurs at the point of maximum azimuth tracking rate and maximum elevation. As the maximum elevation angle approaches 90°, $\dot{V}_{max}$ will eventually exceed the maximum vertical-axis velocity of the antenna, $\dot{S}$.

Fortunately, there is a factor which reduces vertical axis tracking requirement. The antenna has an "on-track" beamwidth,* 2ξ, so that it is possible to track without the antenna pointing directly at the target. We can utilize this "on-track" beamwidth in the following manner. For any satellite path which passes within ξ degrees of zenith, it is possible to switch tracking modes without any interruption in communications. This situation is illustrated in Fig. 14, where V_1, V_2 tracking modes near one of the switchover points are plotted as a function of time for an assumed beamwidth of 0.2 degrees, a maximum satellite elevation angle, $E_{max} = 89.9°$, and a satellite altitude of 6000 miles (circular equatorial orbit). The solid lines show the vertical axis angle if the satellite is on boresight. The two pairs of dashed lines represent the allowable variation in the vertical axis pointing angle due to the beamwidth of the antenna. If the vertical axis angle is anywhere within the area between the dashed lines, communications can be maintained with the satellite. Since the tracking areas have a point of intersection at $V = V_s$, a smooth transition between tracking modes is possible without a lapse in communications. For satellite tracks where $E_{max} > 89.9°$, the two tracking mode areas will have a large area of intersection rather than a single point of intersection as in the limiting case discussed above.

This operation of switching tracking modes will be referred to as the "switch-mode." If the switch mode is employed, the vertical axis is to

* That is, the beamwidth for which the signal-to-noise ratio at the receiver is considered sufficient for communication objectives of the system.

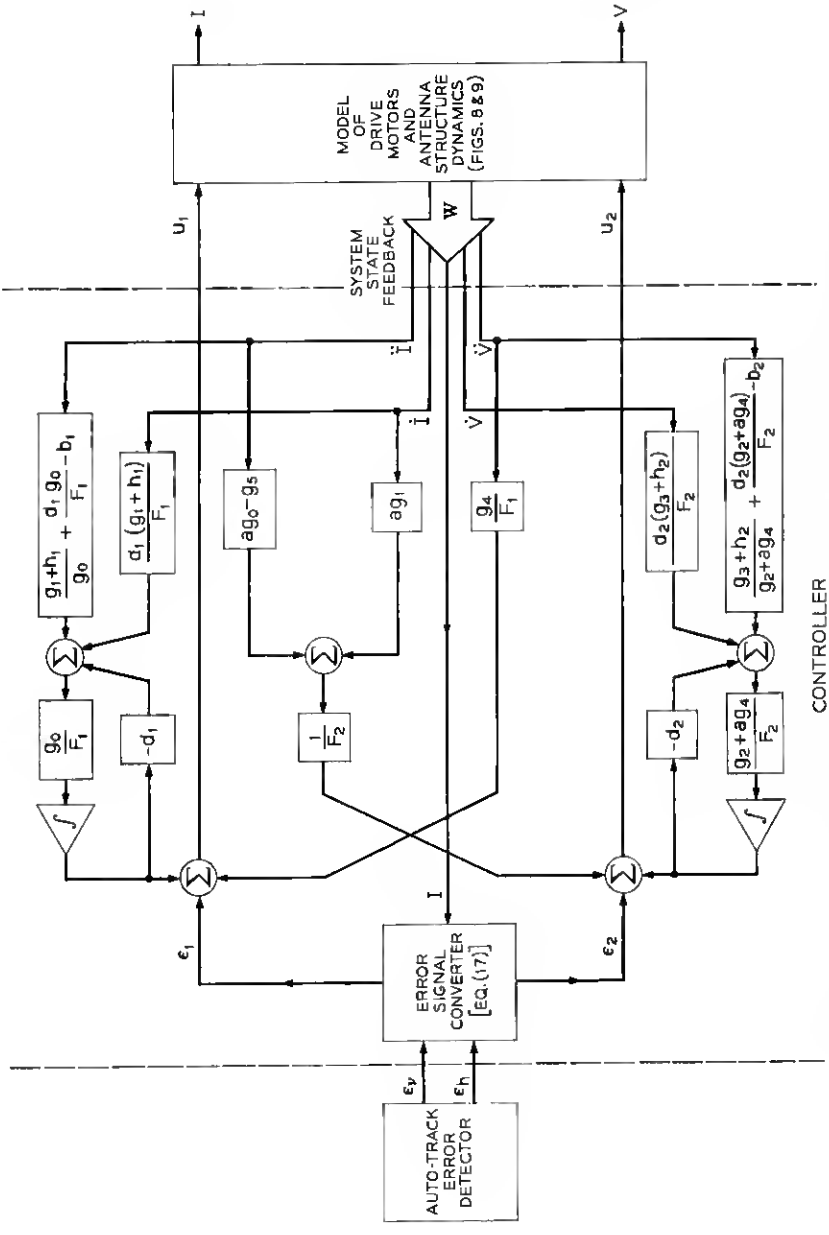

Fig. 12 — Detail structure of basic controller design for normal autotrack mode.

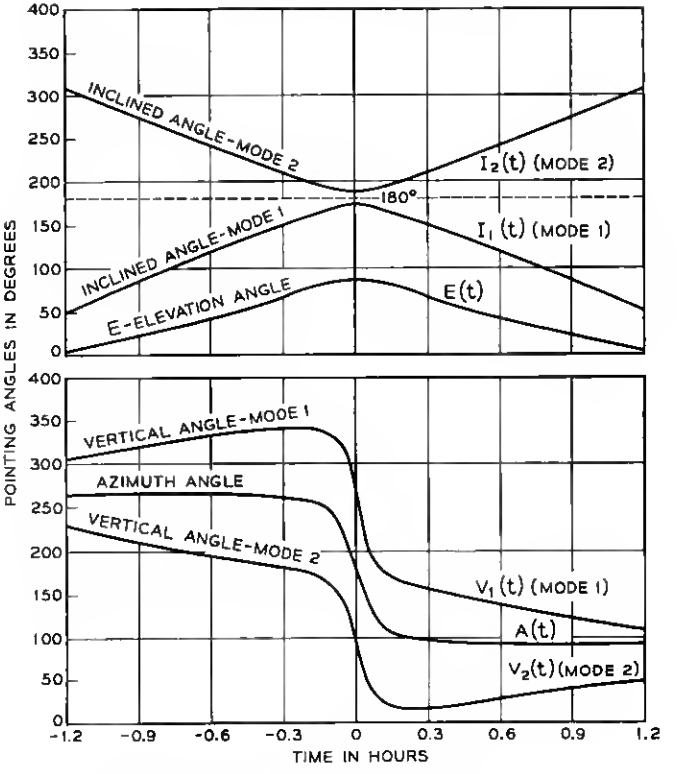

Fig. 13 — Antenna pointing angles for satellite in circular equatorial orbit of 6000 mile altitude with antenna station at 2° latitude.

track keeping the satellite on boresight until, at time t_{s1} in Fig. 14, the vertical axis angle of the tracking mode equals the angle at which switchover from one mode to the other will occur. This switchover angle, V_s, is equal to the azimuth angle at the maximum elevation point and is computed in advance from the predicted satellite orbit. At t_{s1}, a vertical error signal $(V_s - V)$ is employed to keep the vertical axis angle at V_s. This error signal $(V_s - V)$ is maintained until, at time t_{s2} as in Fig. 14, the vertical axis angle for boresight tracking of the second tracking mode is equal to V_s. At this point the switch mode vertical axis error $(V_s - V)$ is replaced by the boresight tracking error $(V_r - V)$ and tracking is continued using the second tracking mode.

Graphical investigation of this switchover process indicates that, depending on the satellite track, a particular tracking mode should be

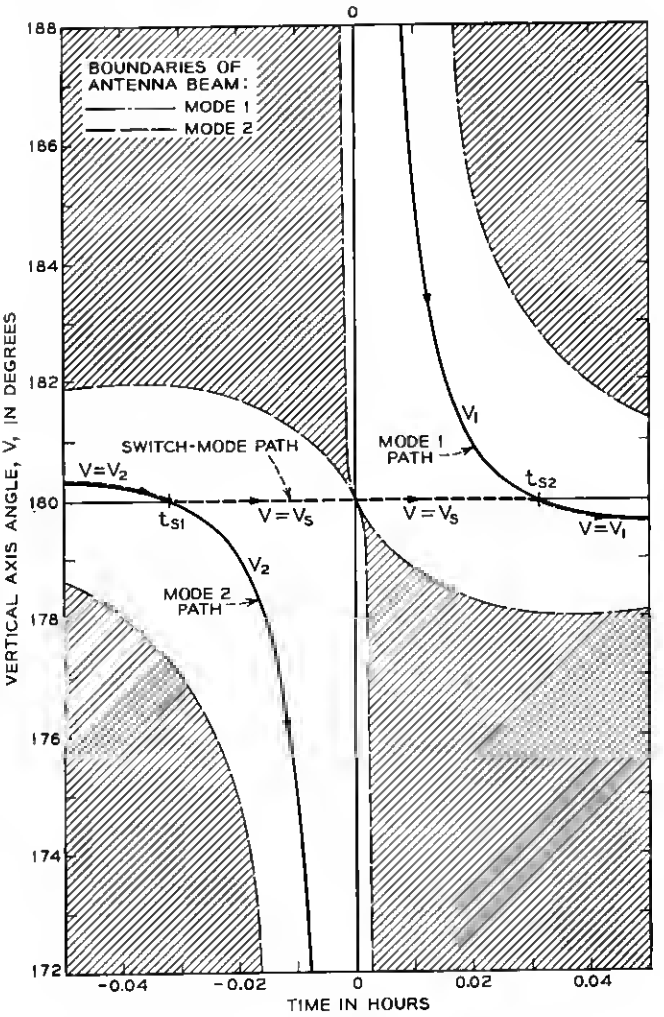

Fig. 14 — Tracking angles of vertical axis near one of the switchover points for $E_{max} = 89.9°$, $\xi = 0.1°$, and 6000 mile circular equatorial orbit.

chosen for tracking from the horizon, where the satellite is first acquired, to the maximum elevation point and the other mode from the maximum elevation to the horizon. The choice is made by determining, from orbit predictions, the initial vertical axis angular velocity for each tracking mode when the satellite initially appears at the horizon. If the initial vertical axis tracking velocity of mode 1, $\dot{V}_{H1}$, is greater than the initial

tracking velocity of mode 2, $\dot{V}_{H2}$, then mode 1 is used first and the switch-over is made to mode 2. The opposite procedure is employed if $\dot{V}_{h2} > \dot{V}_{h1}$. Although the tracking velocity requirement is greater at the horizon using this procedure, the tracking velocity requirements near zenith are reduced.

For satellite tracks where $E_{max} < 90° - \xi$, one cannot switch tracking modes without losing communications for a brief period. Therefore, one desires to track the satellite hy remaining in the same tracking mode. However, instead of pointing directly at boresight when tracking the satellite, one can again utilize the "on-track beamwidth" to point off boresight and still be within the antenna beam as shown in Fig. 15. By following the tracking path, $\tilde{\Gamma}$, illustrated in Fig. 15, it is possible to significantly reduce the peak vertical axis velocity requirement from the velocity required for boresight tracking. Tbis procedure will subsequently be referred to as the "slant-through" mode.

In the design of tbe antenna drive system, an upper limit is needed on the maximum vertical axis angular velocity required to follow the slant-through path, $\tilde{\Gamma}$, for all circular satellite orbits of a given altitude, i.e. the worst case slant-through speed, $\hat{S}$. Since it is expected that the com-

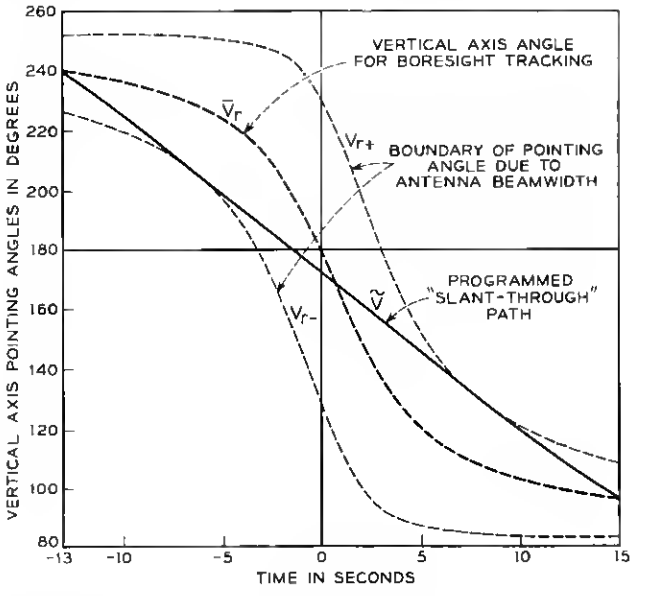

Fig. 15 — "Slant through" path for 6000 mile altitude, circular polar orbit with $E_{max} = 89.893°$.

munication satellites to be tracked will be launched in the same direction as the earth's rotation, the worst case will occur when the inclination angle, α, equals 90° (a polar circular orbit) and $E_{\max} = (90° - \xi)$. (This elevation is chosen since if $E_{\max}$ is larger than $(90° - \xi)$ the switch mode will be employed.) An approximate expression for $\hat{S}$ is derived in Appendix C. Shown in Fig. 16 is a graph of $\hat{S}$ as a function of satellite altitude, $x = (r - 1)$, for antenna half-beamwidths of 0.1° and 0.2°. For example, the continuous tracking of satellites in nearly circular orbits of 6000 miles altitude with an antenna half-beamwidth of 0.1° would require a vertical axis slewing capability of approximately 1 rpm. A major factor affecting this capability is the gear ratio used in the drive system, the choice of which depends also on other important considerations such as tracking performance at very low speeds, immunity to disturbance torques, minimization of reflected load inertia, and drive power requirements.

This tracking capability should not be difficult to achieve for medium and high altitude satellite systems. For low altitude systems, continuous tracking may be achieved with tbe same speed capability by temporarily

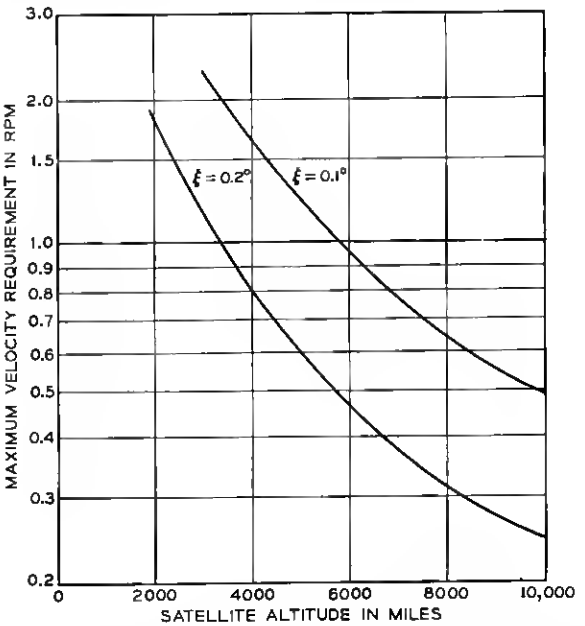

Fig. 16 — Vertical axis velocity requirement as a function of satellite altitude for antenna half-beamwidths $\xi = 0.1°$ and 0.2°.

broadening the antenna beam during the near-zenith portion when signal strength conditions are favorable.

The slant-through mode can be performed by biasing the vertical axis error signal with another signal $(\bar{V} - \bar{V}_r)$ between $t_1 < t < t_2$ as shown in Fig. 15. $\bar{V}$ is the computed vertical axis angle which will program the "slant-through" path within the antenna beamwidth. $\bar{V}_r$ is the computed vertical axis angles for boresight tracking determined from orbit predictions. Since $\bar{V}_r \doteq V_r$, the resultant error signal looks like $(\bar{V} - V)$.

The above discussion indicates the following tracking strategy. From orbit predictions of the satellite path, the elevation values (E) as a function of time are scanned. If the maximum elevation, $E_{\max}$, is greater than or equal to $(90° - \xi°)$ the "switch" mode will be employed as explained above. If $E_{\max} < (90° - \xi)$, but $(\dot{V}_{\max}) > \hat{S}$, the slant-through mode is employed at time t_1 in Fig. 15. If neither of these special modes is required, normal tracking will be employed. For the normal and slant-through modes, it is desirable to use the tracking mode which has the smaller vertical axis velocity required when initially acquiring the satellite at the horizon. The inclined axis velocity requirement at satellite acquisition is the same for either mode. If $\dot{V}_{H2} > \dot{V}_{H1}$, then mode 1 will be used for tracking and the opposite choice will be used if $\dot{V}_{H1} > \dot{V}_{H2}$.

The mode tracking strategy is shown in flow chart form in Fig. 17. Note that no special control signals are needed for the inclined axis. The initial inclined and vertical pointing angles when the satellite appears at the horizon, I_H and V_H, can also be determined from orbit predictions and (8).

V. DESIGN RESULTS AND CONCLUSIONS

The second phase of this design study consists of a simulation and design evaluation program on a hybrid analog-digital computer facility.[7] The major objectives of this program are to verify, improve, and if possible, simplify the basic controller strategy developed in Section IV.

The analog computer portion of the facility is being used for the simulation of the controller and the antenna dynamics. The experimental results discussed here were based on a simulation of an open cassegrain antenna with a 56-foot aperture, an overall height of about 70 feet, and a total weight of about 100 tons,* using two 25-hp hydraulic motors for the vertical axis drive and two 10-hp motors for the inclined axis drive.

The closed-loop response of the antenna drive system using the basic controller design shown in Fig. 12 was tested using step and ramp in-

* Subsequent design modifications have changed the weight and the antenna dynamics somewhat, but not enough to significantly affect the simulation results.

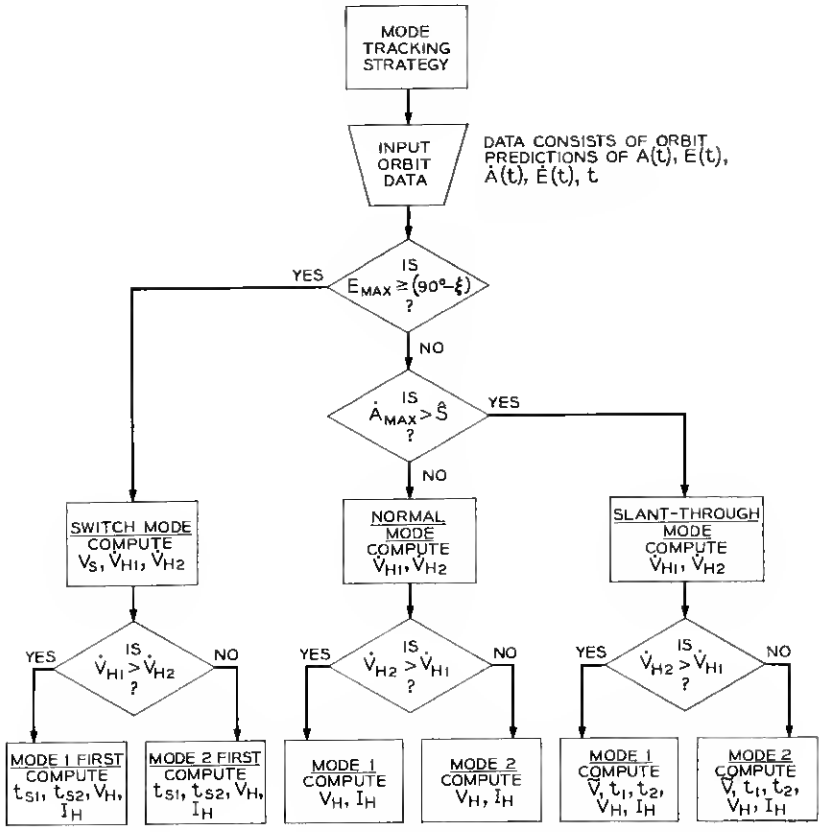

Fig. 17 — Flow chart of tracking strategy.

puts, I_r and V_r, as well as wind disturbance torque inputs. The design for each channel was based on the approximate model transfer function (32) with parameter values, $\eta = 2.4$, $\mu = 1.9$, and a range of values of ω_0 from 5 to 40 sec.$^{-1}$. Because of the low accelerations required for the expected satellite tracks, the constraint (35) was easy to satisfy with the available range of loop gains; therefore the major considerations in the choice of ω_0 were good transient response, steady-state accuracy, and immunity to wind disturbances. Satisfactory performance with respect to the objectives of zero steady-state error in tracking constant velocity inputs and minimum channel interaction was achieved in the experimental design with state feedback gain adjustments close to the nominal values computed for the expressions in Fig. 12.

The experimental data obtained from this design study has established

the feasability of operating the open cassegrain antenna under severe wind conditions without a radome. A series of tests using simulated wind loads corresponding to a 40-mph gale with gusts exceeding 80 mph have indicated that the control system is capable of maintaining the antenna beam on-track with both a mean and rms error less than 0.002 degrees, which is about 1/100th of the nominal beamwidth of the antenna.

The future test program in this design study will employ the digital computer portion of the hybrid computer facility to simulate satellite tracking data, autotrack error detector signals, and the necessary coordinate conversions for resolving the error signal inputs and the angular outputs of the non-orthogonal axes of motion. This will provide a complete simulation of the overall autotrack system shown in Fig. 2, and will allow testing and evaluation of the overall control strategy for non-orthogonal mounts, including the near zenith control modes discussed in Section 4.2.

VI. ACKNOWLEDGMENTS

The authors wish to acknowledge and thank Messrs. J. S. Cook, K. N. Coyne, J. Chernak, J. F. Kaiser, and J. A. Norton for their advice and contributions to this work.

APPENDIX A

We consider the polar coordinates $[r(t),\theta(t)]$ of the satellite in the orbital plane to be given, and then make the sequence of transformations necessary to relate the tracking coordinates (A,E) to these orbit parameters:

A.1 *Transformation from orbit plane to equatorial plane*

We define rectangular coordinates XYZ and $X'Y'Z'$ as shown in Fig. 18, with the X and X' axes coincident with the line formed by the intersection of the orbit and equatorial planes. The satellite moves into the northern hemisphere at the $+X$-axis. We define the following (see Fig. 18):

$r(t)$ = range from center of earth to satellite at time t.
$\theta(t)$ = angle which $r(t)$ makes at time t, measured from the X'-axis.
α = inclination angle of orbit plane with equatorial plane.*

* Should not be confused with antenna incline-angle, α, defined in Section II, since they will not be used in the same context.

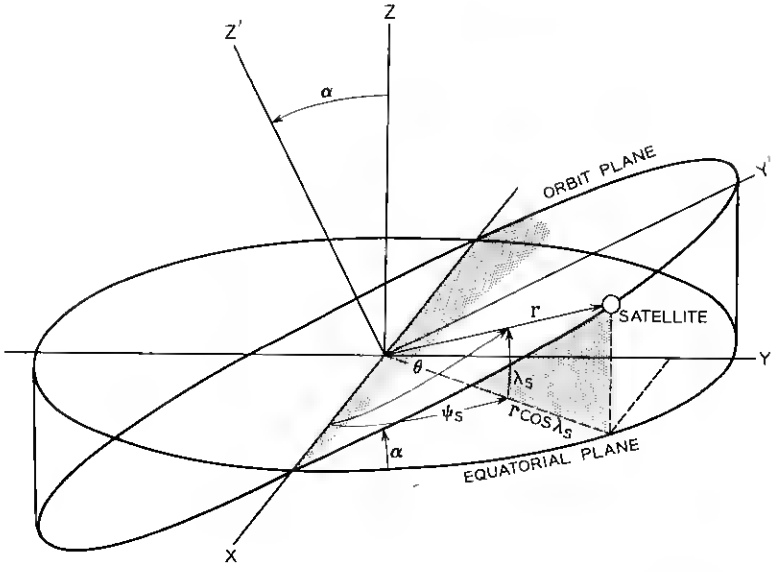

Fig. 18 — Satellite coordinate conversion — Orbit plane to equatorial plane.

$\psi_s(t)$ = longitude angle of satellite eastward from X-axis.
$\lambda_s(t)$ = latitude angle of satellite northward from equator.

The transformation from the orbit plane to equatorial plane corresponds to a rotation about the X-axis through an angle α, so that

$$\begin{pmatrix} X \\ Y \\ Z \end{pmatrix} = \begin{pmatrix} 1 & 0 & 0 \\ 0 & \cos\alpha & -\sin\alpha \\ 0 & \sin\alpha & \cos\alpha \end{pmatrix} \begin{pmatrix} X' \\ Y' \\ Z' \end{pmatrix} \tag{36}$$

Expressing the rectangular coordinates in the equivalent spherical polar coordinates, we have

$$\begin{pmatrix} r\cos\lambda_s\cos\psi_s \\ r\cos\lambda_s\sin\psi_s \\ r\sin\lambda_s \end{pmatrix} = \begin{pmatrix} 1 & 0 & 0 \\ 0 & \cos\alpha & -\sin\alpha \\ 0 & \sin\alpha & \cos\alpha \end{pmatrix} \begin{pmatrix} r\cos\theta \\ r\sin\theta \\ 0 \end{pmatrix} . \tag{37}$$

A.2 *Transformation from equatorial plane to horizon plane at Antenna Station*

The rectangular coordinates (xyz) are located with the origin at the antenna site as shown in Fig. 19, with the $+x$-axis pointing northward. The notation used here is as follows:

R = radius of the earth (assumed constant)
ψ = longitude angle of antenna site, measured eastward from X-axis
λ = latitude angle of antenna site, measured northward from equator
ρ = slant range to satellite from anetnna site
A = azimuth angle measured CW from x-axis (North)
E = elevation angle measured up from horizon (xy-plane)

The transformation from XYZ coordinates to xyz coordinates can be

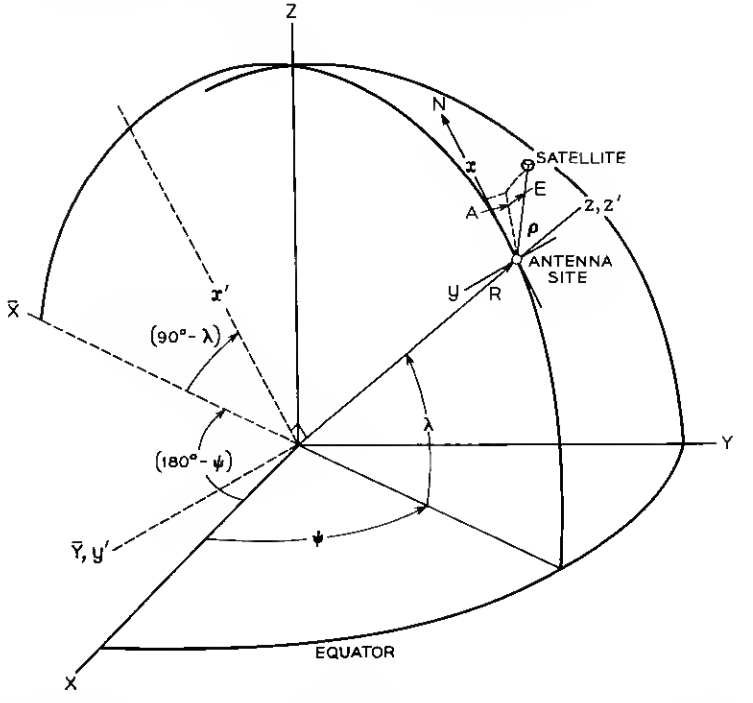

Fig. 19 — Diagram for the transformation of coordinates from the earth-centered system (XYZ) to the local antenna site coordinates (xyz) and pointing angles (A,E).

written as a sequence of two rotations and a translation, as shown in Fig. 19. The first is a CW rotation about the Z-axis through an angle $(180° - \psi)$, which can be written as

$$\begin{pmatrix} \bar{X} \\ \bar{Y} \\ \bar{Z} \end{pmatrix} = \begin{pmatrix} -\cos\psi & -\sin\psi & 0 \\ \sin\psi & -\cos\psi & 0 \\ 0 & 0 & 1 \end{pmatrix} \begin{pmatrix} X \\ Y \\ Z \end{pmatrix}. \tag{38}$$

The second is a CW rotation about the $\bar{Y}$-axis through an angle $(90° - \lambda)$ as indicated in Fig. 19:

$$\begin{pmatrix} x' \\ y' \\ z' \end{pmatrix} = \begin{pmatrix} \sin\lambda & 0 & \cos\lambda \\ 0 & 1 & 0 \\ -\cos\lambda & 0 & \sin\lambda \end{pmatrix} \begin{pmatrix} \bar{X} \\ \bar{Y} \\ \bar{Z} \end{pmatrix}. \tag{39}$$

Thirdly, a simple translation along $+z'$-axis a distance R gives,

$$\begin{pmatrix} x \\ y \\ z \end{pmatrix} = \begin{pmatrix} x' \\ y' \\ z' \end{pmatrix} - \begin{pmatrix} 0 \\ 0 \\ R \end{pmatrix}$$

or, in terms of the spherical coordinates at the antenna site

$$\begin{pmatrix} \rho\cos E\cos A \\ -\rho\cos E\sin A \\ \rho\sin E \end{pmatrix} = \begin{pmatrix} x' \\ y' \\ z' \end{pmatrix} - \begin{pmatrix} 0 \\ 0 \\ R \end{pmatrix}. \tag{40}$$

Finally, combining (37) through (40), we have

$$\begin{aligned} \rho\cos E\cos A &= -r(\sin\lambda\cos\psi\cos\theta + \cos\alpha\sin\lambda\sin\psi\sin\theta \\ &\quad - \sin\alpha\cos\lambda\sin\theta) \\ -\rho\cos E\sin A &= r(\sin\psi\cos\theta - \cos\alpha\cos\psi\sin\theta) \\ \rho\sin E &= r(\cos\lambda\cos\psi\cos\theta + \cos\alpha\cos\lambda\sin\psi\sin\theta \\ &\quad + \sin\alpha\sin\lambda\sin\theta) - R. \end{aligned} \tag{41}$$

Separating these variables gives the desired transformations:

Slant range to satellite:

$$\rho = [r^2 + R^2 - 2rR(\cos\lambda\cos\psi\cos\theta + \cos\alpha\cos\lambda\sin\psi\sin\theta + \sin\alpha\sin\lambda\sin\theta)]^{\frac{1}{2}} \tag{42}$$

Azimuth angle to satellite:

$$A = \tan^{-1}\left(\frac{\sin\psi\cos\theta - \cos\alpha\cos\psi\sin\theta}{\sin\lambda\cos\psi\cos\theta + \cos\alpha\sin\lambda\sin\psi\sin\theta - \sin\alpha\cos\lambda\sin\theta}\right) \tag{43}$$

Elevation Angle to satellite:

$$E = \sin^{-1}\left\{\frac{r(\cos\lambda\cos\psi\cos\theta + \cos\alpha\cos\lambda\sin\psi\sin\theta + \sin\alpha\sin\lambda\sin\theta) - R}{[r^2 + R^2 - 2rR(\cos\lambda\cos\psi\cos\theta + \cos\alpha\cos\lambda\sin\psi\sin\theta + \sin\alpha\sin\lambda\sin\theta)]^{\frac{1}{2}}}\right\} \tag{44}$$

where $-\pi/2 \leqq E \leqq \pi/2$.

In these expressions the constant factors are the orbit inclination angle, α, the antenna site latitude, λ, and the earth radius R. The antenna site longitude angle, ψ, can be considered constant if the effect of the earth's rotation is neglected, but more generally it will have the form

$$\psi(t) = \psi_0 + \Omega t \tag{45}$$

where Ω = earth's angular velocity = $(\pi/12)$ rad/hr. To simplify the expressions we shall measure distance in units of earth radius (e.r.) so that

$$R = 1 \text{ e.r.} \tag{46}$$

Further, to emphasize the constants, let

$$\left.\begin{aligned} C_\alpha &\equiv \cos\alpha, & C_\lambda &\equiv \cos\lambda \\ S_\alpha &\equiv \sin\alpha, & S_\lambda &\equiv \sin\lambda \end{aligned}\right\} \tag{47}$$

Using the notation of (45), (46) and (47), the tracking angles can be written

$$A = \tan^{-1}\left\{\frac{\sin\psi\cos\theta - C_\alpha\cos\psi\sin\theta}{S_\lambda(\cos\psi\cos\theta + C_\alpha\sin\psi\sin\theta) - S_\alpha C_\lambda\sin\theta}\right\} \tag{48}$$

$$E = \sin^{-1}\left\{\frac{r(C_\lambda(\cos\psi\cos\theta + C_\alpha\sin\psi\sin\theta) + S_\alpha S_\lambda\sin\theta) - 1}{[1 + r^2 - 2r(C_\lambda(\cos\psi\cos\theta + C_\alpha\sin\psi\sin\theta) + S_\alpha S_\lambda\sin\theta)]^{\frac{1}{2}}}\right\} \tag{49}$$

where r, θ, and ψ are in general varying with time. The denominator in (49) is the range from antenna to satellite in units of earth radii. The numerator in (49) gives the necessary condition for the satellite to be above the horizon at the antenna site, namely:

$$r[C_\lambda\ (\cos\psi\ \cos\theta + C_\alpha \sin\psi\ \sin\theta) + S_\alpha S_\lambda \sin\theta] \geqq 1 \Rightarrow E > 0 \qquad (50)$$

where, of course, r is the radius vector of the satellite in units of earth radii.

During the period when (50) is satisfied, the $A(t)$ and $E(t)$ given above, as well as their time derivatives, give the required information to evaluate the antenna drive angles and rates, from (8) and (10) in Section II. For non-circular orbits, the expressions for (r,θ) as functions of time must still be determined, and in general a computer routine[4] would be used. The main usefulness of the analytical expressions (48) and (49) is in estimating tracking requirements for particular orbits where complete data are not needed.

A.3 *Tracking angles and rates for circular orbits*

For a given inclination angle, α, of the circular orbit plane (see Fig. 18), and a given latitude, λ, of the antenna site, the tracking angles $A(t)$ and $E(t)$ can be obtained from (48) and (49) as explicit functions of time by substituting the time functions $\psi(t)$, given in (45), and

$$\theta = \omega t + \theta_0 \qquad (51)$$

where $\theta_0 = \theta(t)$ at arbitrary time reference, $t = 0$, and the constant angular velocity of the satellite is given by

$$\omega = kr^{-3/2} \qquad (52)$$

where

$$\begin{aligned} r &= 1 + h/R, \\ h &= \text{satellite altitude} \\ R &= \text{earth radius} \\ k &= (g/R)^{\frac{1}{2}} \\ g &= \text{accel. due to gravity} \end{aligned}$$

or

$$k \doteq 4.47\ \text{hr}^{-1} \doteq 1.24 \times 10^{-3}\ \text{sec}^{-1}.$$

The particular case of the *circular equatorial orbit* yields the simplest expressions for azimuth and elevation angles and rates. Letting $\alpha = 0$,

we obtain from (48) and (49) the angle expressions:

$$[A(t)]_{\alpha=0} \equiv A^*(t) = \tan^{-1}\left\{-\frac{\tan\varphi(t)}{\sin\lambda}\right\} \tag{53}$$

$$[E(t)]_{\alpha=0} \equiv E^*(t) = \sin^{-1}\left\{\frac{r\cos\lambda\cos\varphi(t) - 1}{[1 + r^2 - 2r\cos\lambda\cos\varphi(t)]^{\frac{1}{2}}}\right\} \tag{54}$$

where

$$\varphi(t) = (\omega - \Omega)t + \theta_0 - \psi_0 . \tag{55}$$

Taking the time derivative of (53), the azimuth *rate* for circular equatorial orbits is

$$[\dot{A}(t)]_{\alpha=0} \equiv \dot{A}^*(t) = \frac{-\sin\lambda}{\sin^2\varphi(t) + \sin^2\lambda\cos^2\varphi(t)}\,\dot{\varphi} \tag{56}$$

where, from (55), $\dot{\varphi} = \omega - \Omega =$ constant *relative* angular velocity of the satellite with respect to the earth. The maximum azimuth *rate* occurs when $\varphi(t) = 0$, and is given by†

$$|\dot{A}_{\max}{}^*| = \frac{(\omega - \Omega)}{\sin\lambda} \tag{57}$$

where, from (45) and (52),

$$\dot{\varphi} = (\omega - \Omega) \doteq 4.47\, r^{-3/2} - (\pi/12)\ \text{rad/hr} \tag{58}$$

the maximum elevation, E, also occurs when $\varphi(t) = 0$, and has the value,

$$E_{\max}{}^* = \sin^{-1}\left\{\frac{r\cos\lambda - 1}{[1 + r^2 - 2r\cos\lambda]^{\frac{1}{2}}}\right\}. \tag{59}$$

Differentiating (54), the elevation *rate* for the case of circular equatorial orbits is,

$$\dot{E}^*(t) = \frac{-r\cos\lambda\sin\varphi(t)\,(r - \cos\lambda\cos\varphi(t))\,\dot{\varphi}}{(1 - \cos^2\lambda\cos^2\varphi(t))^{\frac{1}{2}}(1 + r^2 - 2r\cos\lambda\cos\varphi(t))}, \tag{60}$$

where $\varphi(t)$ and and $\dot{\varphi}$ are given by (55) and (58), respectively. We are interested in the maximum value of $\dot{E}$ when the satellite is visible, i.e. when $r\cos\lambda\cos\varphi(t) > 1$. Once the parameters r and λ have been specified, this can be determined from (60).

† If $I = 180°$, then $\dot{V}_{\max} = \dot{A}_{\max}$.

APPENDIX B

We derive the inclined and vertical channel error signals as functions of the waveguide error signals and the controlled antenna angles (I,V) in this appendix. The desired error signals are

$$\begin{aligned} \epsilon_1 &\triangleq I_r - I \\ \epsilon_2 &= V_r - V . \end{aligned} \tag{61}$$

Since we desire to make $\epsilon_1(t)$ to be within some small specified tolerance, we assume

$$\sin \tfrac{1}{2}(I_r - I) \doteq \epsilon_1/2$$

and (62)

$$\sin \tfrac{1}{2}(I_r - I) \doteq \sin I.$$

Using (62) and the trigonometric identity,

$$\sin \tfrac{1}{2}(A + B) \sin \tfrac{1}{2}(A - B) = -\tfrac{1}{2}(\cos A - \cos B),$$

we can write

$$\epsilon_1 = \frac{(\cos I - \cos I_r)}{\sin I} . \tag{63}$$

Using (8) and (63), one obtains

$$\epsilon_1 \doteq \frac{(\sin E_r - \sin E)}{b^2 \sin I} . \tag{64}$$

Using (1), the trigonometric identity for the difference between $\sin E_r$ and $\sin E$, and assumptions similar to those used above

$$\epsilon_1 = \frac{(E_r - E) \cos E}{b^2 \sin I} = \frac{\epsilon_v \cos E}{b^2 K_v \sin I} . \tag{65}$$

From (7) and some algebraic manipulation, we can write (65) as

$$\epsilon_1 = \frac{\epsilon_v}{K_v}\left[1 + a^2 \cot^2\left(\frac{I}{2}\right)\right]. \tag{66}$$

The vertical-axis error signal, ϵ_2 is found using a similar procedure. From (61) and (8),

$$\epsilon_2 = (V_r - V) = A_r - \Delta(I_r) - A + \Delta(I). \tag{67}$$

From (1), we have

$$\epsilon_2 = \frac{\epsilon_h}{K_h \cos E} + \Delta(I) - \Delta(I_r). \tag{68}$$

Using the trigonometric identity,

$$\tan \Delta(I_r) - \tan \Delta(I) = \frac{\sin (\Delta(I_r) - \Delta(I))}{\cos \Delta(I_r) \cos \Delta(I)} \tag{69}$$

and, assuming that for normal tracking $(\Delta(I_r) - \Delta(I))$ is small, we obtain

$$\begin{aligned} \Delta(I_r) - \Delta(I) = \tfrac{1}{2}[&\tan \Delta(I_r) - \tan \Delta(I)] \\ &\times \{\cos [\Delta(I_r) + \Delta(I)] \\ &+ \cos [\Delta(I_r) - \Delta(I)]\} \end{aligned} \tag{70}$$

using (69) and the trigonometric identity for the product of two cosines. Using (7) and assuming that

$$\begin{aligned} -\frac{1}{a}\left[\tan\left(\frac{I_r}{2}\right) = \tan\left(\frac{I}{2}\right)\right] &\doteq -\frac{\epsilon_1}{a[1 + \cos I]} \\ \cos [\Delta(I_r) - \Delta(I)] &\doteq 1 \\ \cos [\Delta(I_r) + \Delta(I)] &\doteq \cos 2\Delta(I) \end{aligned} \tag{71}$$

(70) becomes

$$\Delta(I_r) - \Delta(I) \doteq -\frac{\epsilon_1}{2}[1 + \cos 2\Delta(I)][1 + \cos I]^{\frac{1}{2}}. \tag{72}$$

After some additional algebraic manipulation using (7) and trigonometric identities, one obtains

$$\Delta(I_r) - \Delta(I) \doteq -a\epsilon_1[1 - \sin E]^{-1}. \tag{73}$$

Using (68) and (7), (73) becomes

$$\epsilon_2 = \frac{\epsilon_h}{K_h}\left\{b^2 \sin^2 I\left(1 + a^2 \cot^2 \frac{I}{2}\right)\right\}^{-1} + \frac{a\epsilon_v}{2K_v} \csc^2\left(\frac{I}{2}\right). \tag{74}$$

APPENDIX C

An approximate expression for $\hat{S}$ is derived in this appendix. Referring to Fig. 20, one can say

$$\sin [(\pi/2) - \xi] = [r \cos \psi_0 - 1][(r \cos \psi_0 - 1)^2 + (r \sin \psi_0)^2]^{-\frac{1}{2}} \tag{75}$$

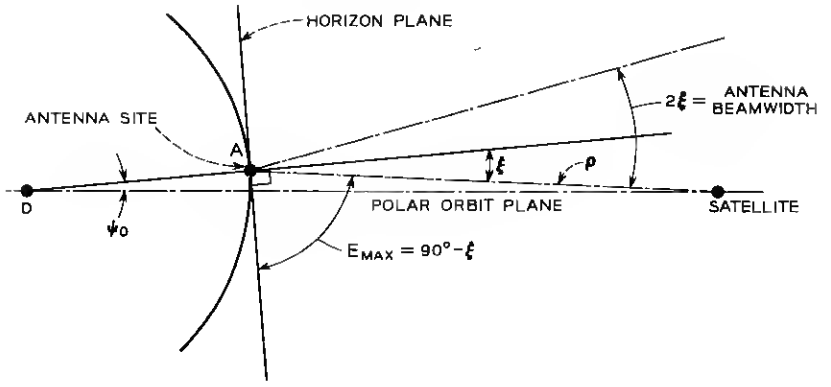

Fig. 20 — Tracking geometry for worst case slewing speed calculation.

Since ξ and ψ_0 are small angles, (75) can be written as

$$1 - \frac{\xi^2}{2} = \left[1 - \frac{r\psi_0^2}{2(r-1)}\right]\left[1 + \frac{r\psi_0^2}{(r-1)^2}\right]^{-\frac{1}{2}}. \tag{76}$$

Since $r\psi_0^2/(r-1)^2 \ll 1$, then (76) can be expressed in the form

$$\xi^2 = \frac{r\psi_0^2}{(r-1)} + \frac{r\psi_0^2}{(r-1)^2} + \cdots \tag{77}$$

where the remaining terms of the series are negligible compared to the first two terms in (77). Solving (77) for ξ,

$$\xi \doteq \frac{r\psi_0}{(r-1)}$$

or

$$\psi_0 \doteq \frac{(r-1)}{r}\,\xi. \tag{78}$$

Using (48), (49), (8) and (78) for the special case of a circular polar orbit of 6000 mile altitude ($r = 2.5$ e.r.) and $\xi^\circ = 0.1°$, the vertical axis angle pointing directly at the satellite and boundaries on either side of the vertical axis angle which are allowable for tracking of the satellite were graphically determined and plotted in Fig. 15. The maximum velocity requirement, $\hat{S}$, was graphically determined by picking the minimum slope as shown in Fig. 15. For the particular example plotted,

$$\hat{S} \doteq 1 \text{ R.P.M.} \tag{79}$$

The velocity requirement for "boresight tracking," $\tilde{S}$, is obtained by taking the time derivative of (48) with $S_\alpha = C_\lambda = 1$ and evaluating at $t = 0$. The result is

$$\tilde{S} = | \dot{V}_{\max} |_{\alpha=90^\circ} \doteq \omega/\psi_0 \tag{80}$$

for small ψ_0 angles. Using equation (78), one can write

$$\tilde{S} = \frac{r\omega}{(r-1)\xi}. \tag{81}$$

Using (81) for a 6000 mile polar circular orbit, the comparable slewing requirement for "boresight tracking" is 2.85 rpm. Graphical plots for other orbit inclinations, altitudes, and antenna beamwidth angles indicate that tracking on the "edge of the antenna beamwidth," as illustrated in Fig. 15, reduces the required slewing capability for a given circular orbit by approximately $\frac{1}{3}$. Therefore, an approximate expression for $\hat{S}$ is

$$\hat{S} \doteq \tfrac{1}{3}\tilde{S}. \tag{82}$$

Using (81) and (52), (82) can be expressed as

$$\hat{S} \doteq \frac{2.3 \text{ R.P.M.}}{r^{\frac{1}{2}}(r-1)\xi^\circ} \tag{83}$$

where r is in earth radii and ξ°, the half-beamwidth angle, is in degrees.

REFERENCES

1. Cook, J. S., et al., The Open Cassegrain Antenna: Part I, Electromagnetic Design and Analysis, B.S.T.J., this issue, pp. 1255–1300.
2. Cook, J. S., and Lowell, R., The Autotrack System, B.S.T.J., *43*, July 1963, pp. 1283–1308.
3. Norton, J. A., Tracking Characteristics of a Conic Mount, Part 1, (Structural Analysis Series, SA-15), Unpublished work.
4. Claus, A. J., et. al., Orbit Determination and Prediction, and Computer Programs, B.S.T.J., *42*, July 1963, pp. 1357–1382.
5. Coyne, K. N., Open Cassegrain Antenna — Mathematical Model of Mechanical System, Unpublished work.
6. Lozier, J. C., Norton, J. A., and Iwama, M., The Servo System for Antenna Positioning, B.S.T.J. *42*, July 1963, pp. 1253–1281.
7. Semmelman, C. L., Description of Computer Facilities at Murray Hill, Proc. Eastern Simulation Meeting, Bell Telephone Laboratories, Murray Hill, N.J., June 15, 1965.